



# On the Microstructures of Platinum Aluminide Bond Coatings Produced by Different Aluminizing Methods: Effects on the Performance of Thermal Barrier Coatings on Ni-Based Superalloys

H. M. Tawancy<sup>1</sup>

Received: 1 March 2018 / Revised: 9 April 2018 / Accepted: 11 April 2018 / Published online: 23 April 2018  
© Springer Science+Business Media, LLC, part of Springer Nature and ASM International 2018

## Abstract

It is shown that aluminizing of platinum-modified aluminide bond coatings by an external vapor source of aluminum in an open retort (chemical vapor deposition) can substantially enhance the performance of thermal barrier coatings in comparison with aluminizing by an internal vapor source in a closed retort (pack cementation). This is demonstrated by about twofold increase in life as determined from cyclic oxidation tests at 1150 °C. The difference in behavior is explained with reference to variations in the initial microstructure of each bond coating, particularly the platinum distribution and thickness of the interdiffusion zone. However, in both cases, it is found that decohesion of the top ceramic coatings during cyclic oxidation occurs by spallation of the oxides developed by the bond coatings. It is concluded that aluminizing by chemical vapor deposition improves the thermal stability and resistance to oxidation of the bond coating.

**Keywords** Pt-aluminides · Bond coatings · Thermal barrier coatings · Superalloys · Electron microscopy

## Introduction

Diffusion platinum aluminide coatings have gained wide acceptance as reliable protective coatings for gas turbine blades as well as bond coats topped with yttria-stabilized zirconia in a thermal barrier coating (TBC) [1]. Several studies have demonstrated that incorporating Pt into the aluminide coating leads to the formation of purer scale with slower growth rate [1–6]. In practice, the platinum aluminide is produced by two main processes: (i) electrodeposition and diffusion of a 6–8 μm layer of Pt into the turbine blade and (ii) aluminizing to form an Al-rich surface layer [7].

Two aluminizing methods are distinguished: (i) pack cementation or closed retort chemical vapor deposition (CVD) [8, 9] and (ii) open or flowing gas retort or shortly

CVD [8, 10]. A common feature of the two methods is that vapors of aluminum chloride (AlCl<sub>3</sub>) provide the source of the Al. However, the two methods differ in the method by which the Al source is created. In pack cementation, the vapors are locally created by a pack mixture where the blades are immersed. In contrast, blades to be coated by the CVD method are isolated from the pack. The AlCl<sub>3</sub> vapors are created in an external reactor and then transported into the reaction vessel where the blades are contained.

The resistance to oxidation of the bond coating has been shown by many studies to dictate a TBC life [1]. Therefore, this investigation has been conducted to elucidate the influence of the above aluminizing methods on the microstructure of Pt-modified aluminide coatings and their behavior in TBC systems. Two bond coatings with commercial grades have been selected: (i) RT22LT bond coating produced by pack cementation and (ii) Howmet 150 L bond coating produced by the open retort CVD [11] with a substrate of alloy MAR M002DS produced by directional solidification and yttria-stabilized zirconia top-coating. The investigation focuses on comparative thermal stability, oxidation behavior, and TBC life.

✉ H. M. Tawancy  
tawancy@kfupm.edu.sa

<sup>1</sup> Center for Engineering Research, Research Institute, King Fahd University of Petroleum and Minerals, KFUPM Box 1639, Dhahran 31261, Saudi Arabia

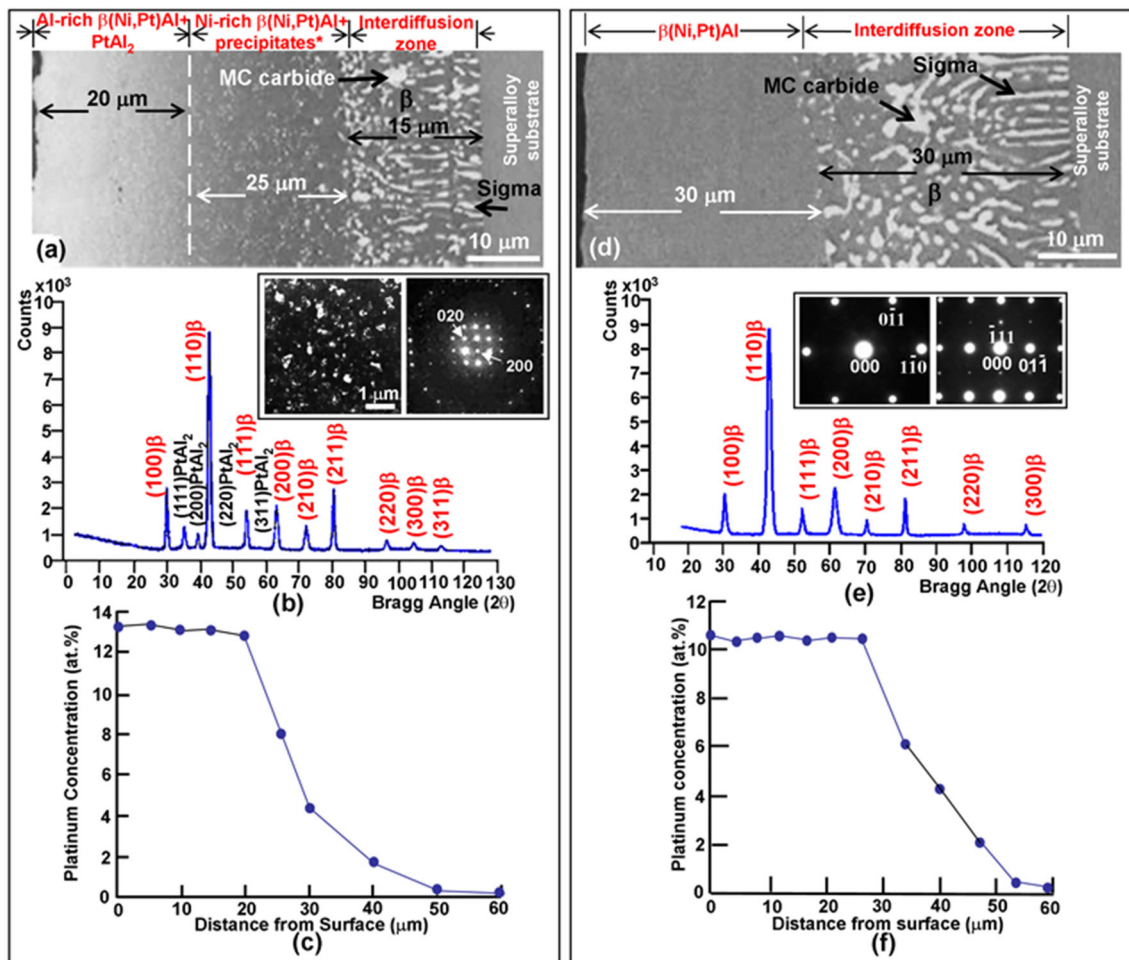


**Fig. 1** Microstructures in the as-deposited condition. (a, d) are backscattered SEM images along the cross sections of RT22LT and Howmet 150 L bond coatings, respectively. (b, e) are x-ray diffractometer traces derived from the surfaces of RT22LT and Howmet 150 L bond coatings, respectively; the insets in (b) show dark-field image of  $\text{PtAl}_2$  particles and the corresponding convergent-beam

microdiffraction pattern in [001] orientation, and the insets in (e) show microdiffraction patterns of  $\beta$ -phase in [111] (left) and [211] (right) orientations. (c, f) are concentration profiles of Pt along cross sections of the RT22LT and Howmet 150 L bond coatings, respectively

## Experimental Procedure

The coatings investigated were deposited on rods (10 cm long and 8 mm diameter) of alloy MAR M002DS with composition of Ni–9.22Co–9.23Cr–9.71W–5.63Al–2.30Ta–1.36Ti–1.64Hf–0.16Mo–0.14C–0.10Fe–0.04Zr–0.01B all in wt.%. The rods were grit-blasted and then ultrasonically cleaned followed by: (i) wet electroplating of Pt layers with nominal thickness of about 7  $\mu\text{m}$  and (ii) diffusion heat treatment for 1 h at 1100 under argon atmosphere according to standard industrial practice [3]. One set of samples was aluminized by the pack cementation method with high Al activity at 850  $^{\circ}\text{C}$  to produce the RT22LT bond coating by inward diffusion of Al, and another set was aluminized by the CVD method with low activity pack at 1100  $^{\circ}\text{C}$  to produce the Howmet 150 L bond coating by outward diffusion of Ni. Some Pt/

aluminized samples were heat-treated at 1150  $^{\circ}\text{C}$  for 3 h under argon atmosphere to produce the characteristic structure of the two bond coatings and reserved for microstructural characterization. The remainder of the Pt-aluminized samples was heat-treated at 1150  $^{\circ}\text{C}$  for 3 h in air to produce the characteristic structure of the two bond coatings and a thin film of  $\text{Al}_2\text{O}_3$  about 1  $\mu\text{m}$  thick to improve the adhesion of the topcoating. Electron beam physical vapor deposition [12] was used to topcoat the Pt-modified aluminides with 250-nm-thick layers of zirconia stabilized by 7 wt.% yttria.

Specimens having 6 mm thickness were prepared from the coated samples for all the tests. The specimens were heated to 1150  $^{\circ}\text{C}$  in a box furnace and cycled to room temperature every 24 h. The life of the TBC system was determined from the average time to spallation of the topcoating in six specimens. Microstructural

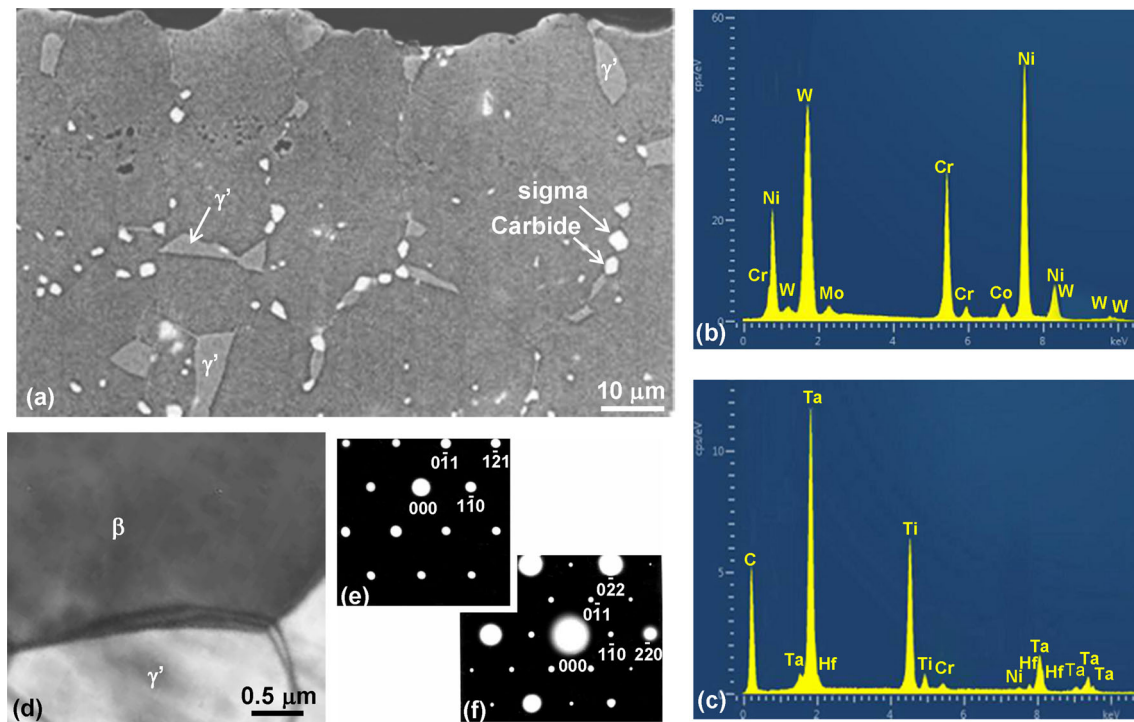


**Fig. 2** Effect of 120 h of exposure at 1150 °C on the microstructure of RT22LT bond coating. (a) Backscattered SEM image along cross section showing secondary precipitates and partial transformation of  $\beta$ -phase into  $\gamma'$ -phase. (b) EDS spectrum showing the elemental composition of the sigma-phase particle marked in (a). (c) EDS spectrum showing the elemental composition of the MC-type carbide

particle marked in (a). (d) Bright-field TEM image near the bond coating surface showing crystals of  $\beta$ - and  $\gamma'$ -phases. (e, f) are the corresponding microdiffraction patterns in [111] orientation of the  $\beta$ - and  $\gamma'$ -phases, respectively; the  $\gamma'$ -phase is distinguished by the characteristic  $L_{12}$  superlattice reflections at  $\{110\}$  positions

characterization techniques included scanning electron microscopy (SEM) with microchemical analysis by energy-dispersive spectroscopy (EDS) and wavelength-dispersive spectroscopy (WDS), x-ray diffractometry, and transmission electron microscopy (TEM). To examine the microstructure in the vicinity of the surface of each bond coating at the higher resolution of TEM, foils were thinned by combination of: (i) electro-polishing on the alloy side using an electrolyte composed of 30 volume% nitric acid in methanol and (ii) ion beam thinning [13]. The foils were investigated using 200 keV microscope.

## Results and Discussion

### As-Deposited Microstructures

Figure 1 illustrates the as-deposited microstructures of the bond coatings. Figure 1a shows that the RT22LT coating consists of two outer layers with total thickness of 45  $\mu\text{m}$  and an inner interdiffusion zone (15  $\mu\text{m}$  thick typically consisting of  $\beta$ -phase containing a mixture of MC-type carbides and sigma phase enriched in heavy transition metals [6, 9]). The x-ray diffractometer trace of Fig. 1b

shows that the surface layers consist of  $\beta$ -phase (cubic B2 superlattice;  $a = 0.29$  nm) with  $\text{PtAl}_2$  as secondary phase (cubic  $\text{CaF}_2$ -type;  $a = 0.59$  nm). Particles of  $\text{PtAl}_2$  are shown in the dark-field TEM image of the inset (left) and corresponding [001] convergent-beam microdiffraction pattern (right). Figure 1c illustrates the variation in Pt concentration across the bond coating layers. It is noted that most of the Pt is present in the outermost 20  $\mu\text{m}$  layer. Since Pt can substitute for Ni in  $\beta$ -NiAl [4], it is evident that excess Pt over the solubility limit is precipitated in the form of  $\text{PtAl}_2$ .

Figure 1d shows that the Howmet 150 L coating consists of one layer about 30  $\mu\text{m}$  thick and 30- $\mu\text{m}$ -thick interdiffusion zone with structure similar to that of RT22LT coating. The corresponding x-ray diffractometer trace of Fig. 1e shows that the coating layer consists only of  $\beta$ -phase as further illustrated by its [111] (left) and [112] (right) characteristic electron diffraction patterns of the inset. Evidently, in this case, Pt is entirely accommodated in solid solution in the  $\beta$ -phase. This is further confirmed in the concentration profile of Fig. 1f where the Pt content is about the same across the outer layer unlike the RT22LT coating (Fig. 1c). As demonstrated below, both the thermal stability and oxidation properties are impacted by the

above-observed differences in microstructures of the RT22LT and Howmet 150 L bond coatings. On the other hand, the thicker interdiffusion zone of Howmet 150 L coating with higher concentration of heavy transition metals such as W and Ta can present a stronger barrier to bond coating degradation by interdiffusion at high temperatures [6, 9] as demonstrated below.

### Thermal Stability Characteristics

Figure 2 shows the microstructure of RT22LT bond coating after 144 h at 1150 °C. The SEM image of Fig. 2a and corresponding EDS spectra (Fig. 2b and c) indicate the presence of precipitates in the outer coating layer including Ni–Cr–W sigma phase (Fig. 2a and b) and MC-type carbide (Fig. 2a and c), where M refers to Ta, Ti, and Hf. It is noted here that the ternary Ni–Cr–W can exist over a wide range of composition [14]. Simultaneously, the  $\beta$ -phase has been partially transformed into the Ni-rich  $\gamma'$ -phase as indicated in Fig. 2a and confirmed by TEM observations. Figure 2d is a bright-field TEM image showing crystals of  $\beta$ - and  $\gamma'$ -phases in the vicinity of the surface as demonstrated by the corresponding diffraction patterns of the B2 ( $\beta$ -phase) and  $L_{12}$  ( $\gamma'$ -phase) superlattices in [111] orientation (Fig 2e and f).

Unlike the above case of RT22LT bond coating, the onset of measurable loss of thermal stability indicated by partial  $\beta$ -phase  $\rightarrow$   $\gamma'$ -phase transformation has been observed in Howmet 150 L bond coating following 408 h of thermal exposure at 1150 °C. This is demonstrated in Fig. 3, which shows the microstructure along a cross section (Fig. 3a) and corresponding x-ray diffractometer trace obtained from the surface (Fig. 3b), where characteristic  $L_{12}$  superlattice reflections are observed in addition to the major reflections of the  $\beta$ -phase.

The superior thermal stability of Howmet 150 L coating in comparison with RT22LT coating is further demonstrated in Fig. 4 showing the functional dependence of Pt concentration across the two bond coatings on time at 1150 °C. Although substantial inward diffusion of Pt in the RT22LT coating is observed (Fig. 4a), the Howmet 150 L has maintained uniform distribution of Pt with very little or no evidence for inward diffusion as shown in Fig. 4b after up to 120 h. Such behavior can be attributed to the difference in initial distribution of Pt across the two bond coatings (Fig. 1c and f), where the Pt concentration

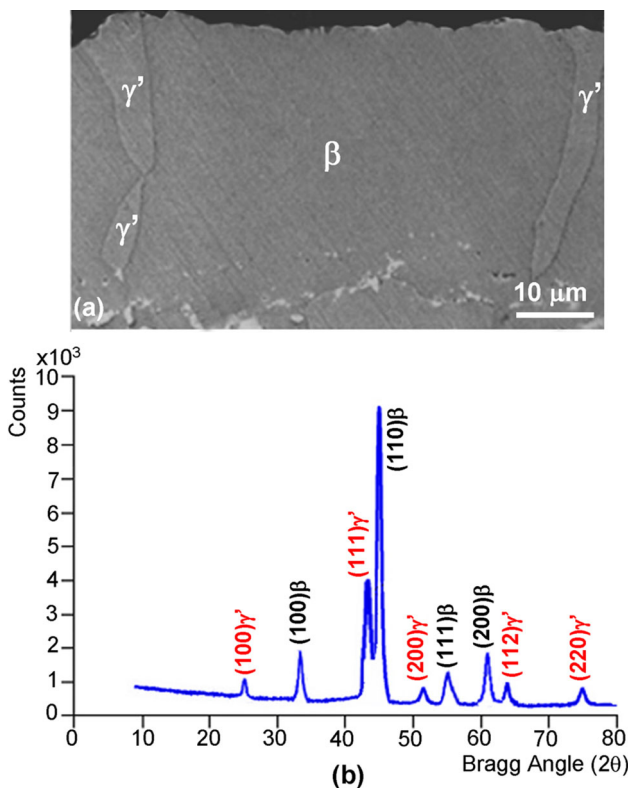


**Fig. 3** Effect of 408 h of exposure at 1150 °C on the microstructure of Howmet 150 L bond coating. (a) Backscattered SEM image along cross section showing partial transformation of  $\beta$ -phase into the  $\gamma'$ -phase. (b) X-ray diffractometer trace derived from the surface showing characteristic Bragg reflections of the  $\beta$ - and  $\gamma'$ -phases

**Fig. 4** Effect of exposure time at 1150 °C on the concentration profiles of Pt as determined by WDS along cross sections of RT22L (a) and Howmet 150 L (b) bond coatings, respectively

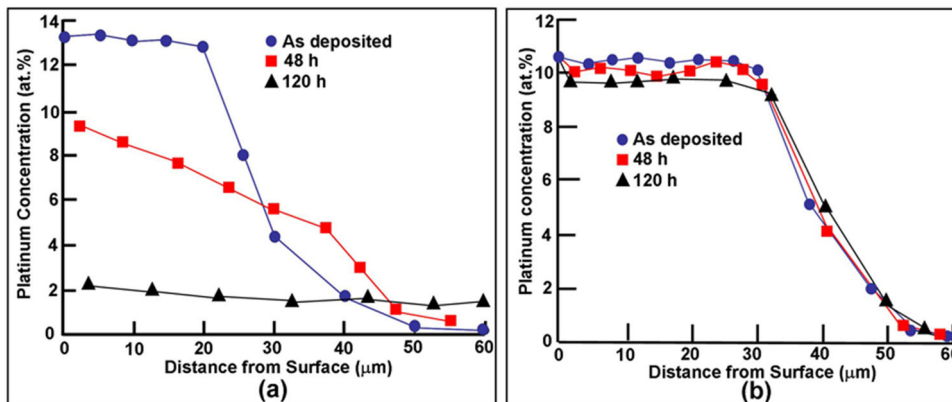
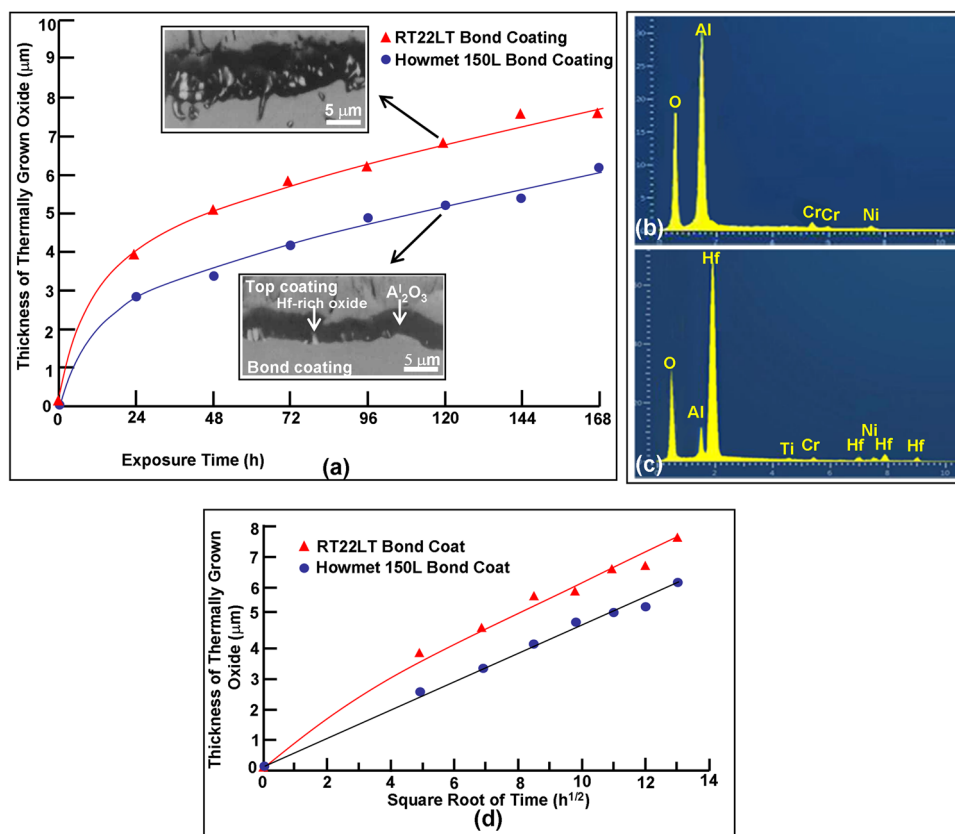


**Fig. 5** Comparative oxidation behavior of RT22LT and Howmet 150 L bond coatings in TBC systems. **(a)** Thickening rates of the thermally grown oxide; the insets are backscattered SEM images along cross sections showing the oxide scales (the dark matrices are  $\text{Al}_2\text{O}_3$  and the bright particles are Hf-rich oxides as indicated by the arrows). **(b, c)** are EDS spectra illustrating the elemental compositions of the matrix oxide in both cases (Al-rich) and secondary particles (Hf-rich). **(d)** Plots of oxide thickness vs. square root of time at 1150 °C showing comparative parabolic behavior of the two bond coatings



gradient in the RT22LT coating is absent in the Howmet 150 L coating. Therefore, upon exposure at elevated temperatures, Pt in the RT22LT coating tends to diffuse inward to eliminate the concentration gradient. Also, the thicker interdiffusion zone of Howmet 150 L bond coating is expected to contribute to its higher thermal stability by reducing the extent of diffusion of substrate elements into the coating.

## Oxidation Behavior

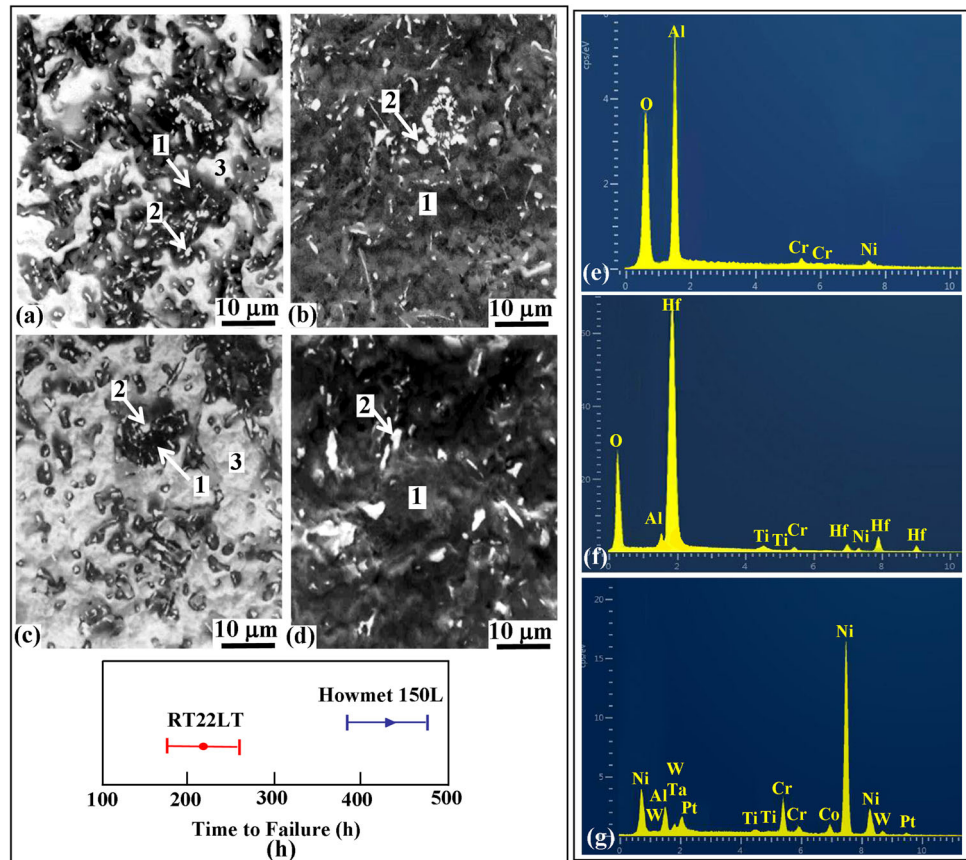
The comparative oxidation behavior of RT22LT and Howmet 150 L bond coatings in TBC systems is illustrated in Fig. 5. Figure 5a shows the oxides thickening rates at 1150 °C as measured from SEM images. As expected from the results of thermal stability described above, the oxide on RT22LT bond coating is observed to grow at a faster rate in comparison with that on Howmet 150 L. The SEM images of inset and corresponding representative EDS spectra of Fig. 5b and c show that the oxide on each bond consists of Al-rich oxide expected to be  $\text{Al}_2\text{O}_3$  with a dispersion oxide pegs enriched in Hf. It is noted that after 120 h of exposure, the Hf-rich oxide has grown deeper into the RT22LT coating, which is known to facilitate further oxidation [15–18]. In contrast, the Howmet 150 L bond coating is observed to remain at an earlier stage of

oxidation with no evidence for internal oxidation, which can be correlated with its higher diffusional stability. Furthermore, Fig. 5d shows that oxidation of Howmet 150 L bond coating closely approaches parabolic rate behavior ( $T = k t^2$ , where  $T$ ,  $k$ , and  $t$  refer to the oxide thickness, oxidation rate constant, and time at a given temperature, respectively), whereas RT22LT bond coating is seen to exhibit some deviation, which correlates with its lower resistance to oxidation.

## Performance of TBC Systems

Experiment shows that the TBC systems investigated are degraded by decohesion of the oxides developed by the two bond coatings leading to spallation of the topcoating. This is demonstrated in Fig. 6. It is observed that the microstructures of the surfaces revealed by decohesion of topcoating in a specimen exposed 240 h at 1150 °C of the system with the RT22LT bond coating (Fig. 6a and b) are similar to those corresponding to the system with the Howmet 150 L bond coating after 408 h (Fig. 6c and d). In both cases, the bond coating surface (Fig. 6a and c) contains islands of  $\text{Al}_2\text{O}_3$  with a dispersion of Hf-rich oxide particles as demonstrated in the representative EDS spectra of Fig. 6e, f, and g. The exposed bottom surfaces of the topcoatings (Fig. 6b and d) are observed to contain a

**Fig. 6** Analysis of surfaces exposed by spallation of the topcoating during cyclic oxidation at 1150 °C. (a, b) are backscattered SEM images showing the microstructures of the RT22LT bond coating surface (a) and bottom surface of topcoating (b) after 240 h. (c, d) are backscattered SEM images showing the microstructures of the Howmet 150 L bond coating surface (c) and bottom surface of topcoating (d) after 408 h. (e, f) are representative EDS spectra illustrating the elemental compositions of the Al-rich oxide and Hf-rich oxide marked 1 and 2, respectively in (a–d). (g) EDS spectrum illustrating the elemental composition of the exposed bond coating surface marked 3 in (a). (h) Comparative lives of TBC systems utilizing the RT22LT and Howmet 150 L bond coatings



continuous layer Al-rich oxide containing a dispersion of Hf-rich oxide particles with corresponding EDS spectra indistinguishable from those shown in Fig. 6e and f. Such observations indicate that fracture of hafnium oxide pegs in the vicinity of the oxide-bond coating interface has played a key role in degradation of the two coating systems. Figure 6g shows the elemental composition of the exposed bond coating surface (regions marked 3 in Fig. 6a and c), which appears to be consistent with  $\gamma$ -phase (Ni-rich solid solution). Evidently, with continued thermal exposure, the  $\beta$ -phase is eventually transformed into  $\gamma$ -phase due to loss of Al and enrichment in Ni caused by oxidation and interdiffusion, respectively.

It is noted here that some earlier studies have demonstrated that excessive growth of oxide pegs enriched in reactive elements such as Hf into the substrate of  $\text{Al}_2\text{O}_3$  formers can degrade its adherence to the substrate due to localized high strain energy [17, 18]. However, as shown in Fig. 6h, the TBC system with Howmet 150 L bond coating outperforms the system with RT22LT bond coating by little less than twofold as determined from the onset of macroscopic spallation of the topcoating during the cycling oxidation tests on 12 specimens from each system. Evidently, this is related to the superior thermal stability and resistance to oxidation of the Howmet 150 L bond coating.

Also, the results indicate that the initial distribution of Pt in the bond coating is a key factor in determining its beneficial effects. In the present case, the results show that partition of Pt into the  $\beta$ -phase and its uniform distribution in the entire coating layer (Howmet 150 L bond coating) are more advantageous than a mixture of  $\beta$ -(Ni, Pt)Al and  $\text{PtAl}_2$  in the outermost coating layer (RT22LT bond coating).

## Conclusions

It is found that an outward Pt-modified aluminide coating aluminized by chemical vapor deposition in an open retort with an external vapor source of Al outperforms an inward coating aluminized by an internal vapor source in a closed retort (pack cementation) in terms of thermal stability and resistance to oxidation. The superior properties of the outward coating are realized in TBC systems by about twofold increase in life as compared to the inward coating. Such difference in behavior of the two coatings is correlated with variations in initial microstructures of the two bond coatings.

**Acknowledgements** The author is grateful for the continued support provided by King Fahd University of Petroleum and Minerals.

## References

1. D.K. Das, Microstructure and high temperature oxidation behavior of Pt-modified aluminide bond coats on Ni-base superalloys. *Prog. Mater. Sci.* **58**, 151–182 (2013)
2. R. Streiff, D.H. Boone, Corrosion resistant modified aluminide coatings. *J. Mater. Eng. Perform.* **22**, 2801–2812 (2013)
3. H.M. Tawancy, L.M. Alhadhrami, Role of platinum in thermal barrier coatings, *J. Eng. Gas Turbines Power Trans. ASME* **132** (2010) article no. 022103
4. B. Gleeson, N. Mu, S. Hayashi, Compositional factors affecting the establishment and maintenance of Al<sub>2</sub>O<sub>3</sub> scale on Ni–Al–Pt systems. *J. Mater. Sci.* **44**, 1704–1710 (2009)
5. H.M. Tawancy, N.M. Abbas, M.O. Aboelfotoh, Effect of platinum on the oxide-to-metal adhesion in thermal barrier coating systems. *J. Mater. Sci.* **43**, 2978–2989 (2008)
6. H.M. Tawancy, N.M. Abbas, T.N. Rhys-Jones, Role of platinum in aluminide coatings. *Surf. Coat. Technol.* **49**, 1–7 (1991)
7. G.W. Goward, Progress in coatings for gas turbine airfoils. *Surf. Coat. Technol.* **108–109**, 73–79 (1998)
8. H.O. Pierson, *Handbook of Chemical Vapor Deposition: Principles, Technology and Applications*, 2nd edn. (Noyes Publications, Norwich, 1999), pp. 110–114
9. P.C. Patnaik, Intermetallic coating for high temperature applications—a review. *Mater. Manuf. Process.* **4**, 133–152 (1989)
10. B.M. Warnes, D.C. Punola, Clean diffusion coatings by chemical vapor deposition. *Surf. Coat. Technol.* **94–95**, 1–6 (1997)
11. S. Bose, *High Temperature Coatings* (Elsevier, Amsterdam, 2007), pp. 88–89
12. H. Lammernann, G. Kienel, PVD coatings for aircraft turbine blades. *Adv. Mater. Process.* **140**, 18–23 (1991)
13. P.J. Goodhew, J. Humphreys, R. Beanland, *Electron Microscopy and Analysis* (Taylor and Francis, New York, 2001), pp. 21–24
14. C.T. Sims, Prediction of phase composition, in *Superalloys II*, ed. by C.T. Sims, N.S. Stoloff, W.C. Hagel (Wiley, New York, 1987), pp. 217–240
15. B.A. Pint, J.A. Haynes, T.M. Besmann, Effect of Hf and Y alloy additions on aluminide coating performance. *Surf. Coat. Technol.* **204**, 3287–3293 (2010)
16. B.A. Pint, K.L. More, I.G. Wright, Effect of quaternary additions on the oxidation behavior of Hf-doped NiAl. *Oxid. Met.* **59**, 257–283 (2003)
17. G. Fisher, P.K. Datta, J.S. Burnell-Gray, W.Y. Chan, J.C. Soares, The effects of active elements additions on the oxidation performance of a platinum aluminide coating at 1100 °C. *Surf. Coat. Technol.* **110**, 24–30 (1989)
18. R. Pendse, J. Stringer, The influence of alloy microstructure on the oxide morphology in a Co–10%Cr–11%Al with and without reactive elements additions. *Oxid. Met.* **23**, 1–16 (1985)